Cerebral Cortex September 2015;25:2863–2875
doi:10.1093/cercor/bhu081
Advance Access publication April 25, 2014

ADF/Cofilin Controls Synaptic Actin Dynamics and Regulates Synaptic Vesicle Mobilization and Exocytosis

Michael Wolf[1,†], Anika-Maria Zimmermann[1,†], Andreas Görlich[1,6,†], Christine B. Gurniak[2], Marco Sassoè-Pognetto[3], Eckhard Friauf[4], Walter Witke[2] and Marco B. Rust[1,5]

[1]Department of Biology, Neurobiology/Neurophysiology Group, University of Kaiserslautern, Kaiserslautern 67663, Germany, [2]Institute of Genetics, University of Bonn, Bonn 53115, Germany, [3]Department of Anatomy, Pharmacology and Forensic Medicine and National Institute of Neuroscience-Italy, University of Turin, Turin 10126, Italy, [4]Animal Physiology Group, University of Kaiserslautern, Kaiserslautern 67663, Germany, [5]Institute of Physiological Chemistry, University of Marburg, 35043 Marburg, Germany and [6]Current address: Rockefeller University, 1230 York Avenue, New York, NY 10065, USA

[†]Michael Wolf, Anika-Maria Zimmermann, and Andreas Görlich contributed equally to this work.

Address correspondence to Marco B. Rust, Institute of Physiological Chemistry, Molecular Neurobiology Group, University of Marburg, Karl-von-Frisch-Straβe 1, Marburg 35032, Germany. Email: marco.rust@staff.uni-marburg.de

Actin is a regulator of synaptic vesicle mobilization and exocytosis, but little is known about the mechanisms that regulate actin at presynaptic terminals. Genetic data on LIMK1, a negative regulator of actin-depolymerizing proteins of the ADF/cofilin family, suggest a role for ADF/cofilin in presynaptic function. However, synapse physiology is fully preserved upon genetic ablation of ADF in mice, and n-cofilin mutant mice display defects in postsynaptic plasticity, but not in presynaptic function. One explanation for this phenomenon is overlapping functions of ADF and n-cofilin in presynaptic physiology. Here, we tested this hypothesis and genetically removed ADF together with n-cofilin from synapses. In double mutants for ADF and n-cofilin, synaptic actin dynamics was impaired and more severely affected than in single mutants. The resulting cytoskeletal defects heavily affected the organization, mobilization, and exocytosis of synaptic vesicles in hippocampal CA3–CA1 synapses. Our data for the first time identify overlapping functions for ADF and n-cofilin in presynaptic physiology and vesicle trafficking. We conclude that n-cofilin is a limiting factor in postsynaptic plasticity, a function which cannot be substituted by ADF. On the presynaptic side, the presence of either ADF or n-cofilin is sufficient to control actin remodeling during vesicle release.

Keywords: CA3–CA1 synapse, hippocampus, neurotransmitter release, presynaptic physiology, synaptic plasticity

Introduction

Actin is the most prominent cytoskeletal protein at synapses, being abundantly present in presynaptic terminals and postsynaptic dendritic spines. A number of studies emphasized the relevance of actin dynamics for spine morphology and postsynaptic plasticity (Cingolani and Goda 2008; Bosch and Hayashi 2011). Pharmacological studies and the subsynaptic distribution of actin filaments (F-actin) suggest a role also in synaptic vesicle mobilization and exocytosis (Fifkova and Delay 1982; Landis et al. 1988; Morales et al. 2000; Korobova and Svitkina 2010). However, very little is known about the mechanisms that link actin dynamics to presynaptic physiology.

Actin dynamics depend on proteins of the ADF/cofilin family that accelerate the dissociation rate of actin subunits and sever F-actin (Bernstein and Bamburg 2010). Two ADF/cofilin isoforms, namely ADF (actin-depolymerizing factor) and n-cofilin (non-muscle cofilin), are highly abundant in the brain (Bellenchi et al. 2007) and both have been localized to synaptic structures (Racz and Weinberg 2006; Herde et al. 2010; Görlich et al. 2011). Studies on hippocampal synapses revealed the relevance of ADF/cofilin for spine morphology (Zhou et al. 2004; Hotulainen et al. 2009; Gu et al. 2010), and a number of upstream regulatory mechanisms have been identified (Tavazoie et al. 2005; Schratt et al. 2006; Zhou et al. 2007; Shi et al. 2009; McNair et al. 2010; Zhou et al. 2012). In agreement, we recently reported impaired spine morphology and postsynaptic plasticity in n-cofilin mutant mice (Rust et al. 2010). Conversely, postsynaptic mechanisms were intact in ADF mutants (Görlich et al. 2011). Genetic manipulation of LIMK1, a negative regulator of ADF/cofilin activity, not only interfered with spine morphology and postsynaptic plasticity, but also with vesicle mobilization and exocytosis (Meng et al. 2002). Accordingly, a role for ADF/cofilin in presynaptic physiology has been hypothesized. Hence, we were surprised to find that presynaptic physiology is fully preserved in ADF and n-cofilin single mutants (Rust et al. 2010; Görlich et al. 2011). The discrepancy between mutant mice for LIMK1 and ADF/cofilin proteins could be explained by 2 scenarios: either ADF and n-cofilin do not function downstream of LIMK1 in presynaptic terminals, or both proteins have overlapping synaptic function. In agreement with the latter scenario, we recently reported elevated n-cofilin levels in synaptic structures of ADF mutants and, vice versa, elevated ADF levels in synaptic structures of n-cofilin mutants (Rust et al. 2010; Görlich et al. 2011). However, LIMK1 interacts with partners others than ADF/cofilin proteins (Yang et al. 2004; Sacchetti et al. 2006; Bernstein and Bamburg 2010), making the first scenario plausible as well.

To examine whether ADF and n-cofilin have overlapping synaptic functions and to test whether ADF/cofilin is relevant for presynaptic physiology, we generated and analyzed double mutant mice. In double mutants, synaptic actin dynamics was severely impaired, stronger than in single mutants. Impaired synaptic actin dynamics in double mutants caused defects in the organization, mobilization, and exocytosis of synaptic vesicles and impaired glutamate release. Our data suggest overlapping functions for ADF and n-cofilin in presynaptic physiology and highlight the importance of ADF/cofilin-dependent actin dynamics in the synapse. We conclude that n-cofilin is the limiting factor in postsynaptic plasticity, whereas the presence of either ADF or n-cofilin is sufficient to drive actin remodeling during presynaptic physiology.

Materials and Methods

Mice

Double mutants that lack ADF and n-cofilin (ACC mice; $ADF^{-/-}$/n-$Cof^{flx/flx,CamKII\text{-}cre}$) were achieved by intercrossing mutants with a single ADF allele and a single floxed n-cofilin allele (Bellenchi et al. 2007). One of the breeding animals additionally expressed cre recombinase under the control of the CaMKIIα-subunit promotor (Minichiello et al. 1999; Rust et al. 2010). In all experiments, age-matched $ADF^{+/+}$/n-$Cof^{flx/flx}$ mice served as controls (called CTR throughout the paper). CaMKII-cre mice were also intercrossed with Rosa26 cre reporter mice to determine cre activity in the hippocampus (Soriano 1999).

Ethics Statement

The treatment of mice was in accordance with the German law for conducting animal experiments and followed the NIH guide for the care and use of laboratory animals. Killing of mice for tissue analysis was approved by the Landesuntersuchungsamt Rheinland-Pfalz (23 177-07/G09-2-001), mouse husbandry and breeding was approved by the City of Kaiserslautern—Referat Umweltschutz.

Synaptosomal Preparation

Synaptosomes from forebrain tissue (cerebral cortex, hippocampus, and striatum) from P40 to P42 mice were isolated as previously described (Dunkley et al. 2008). Briefly, tissue was homogenized and centrifuged at 1000 × *g* for 10 min. Supernatant was separated on discontinuous Percoll gradients (GE Healthcare) by centrifugation for 5 min at 30 000 × *g*. Layers 3 and 4 were collected and washed in sucrose washing buffer (320 mM sucrose, 5 mM Tris; pH 7.4). Forebrain synaptosomes were resuspended in the appropriate buffer and stored on ice until further processing. Protein concentration was determined using a Pierce assay (Thermo Scientific). According to this procedure, we isolated hippocampal synaptosomes that we used for some experiments.

F/G-Actin Ratio

Synaptosomes isolated from forebrain tissue or hippocampus were resuspended in Krebs buffer (in mM: 118.5 NaCl, 4.7 KCl, 1.2 MgCl, 2 $CaCl_2$, 0.1 K_2HPO_4, 5 $NaHCO_3$, 10 glucose, and 20 HEPES), equilibrated at 37 °C for 5 min, and lysed either before or after incubation (3–60 s) in 40 mM KCl solution by adding an equal volume of 2× PHEM extraction buffer (in mM: 120 PIPES, 40 HEPES, 20 EGTA, 4 $MgCl_2$, and 2% Triton X-100; pH 7.0). After protein separation, insoluble proteins were resuspended in an equivalent volume of 1× PHEM buffer, adjusted to that of the supernatant. Thereafter, equal volumes of soluble and insoluble protein fractions were loaded on SDS–PAGE, and actin levels in both protein fractions were quantified by western blotting. For experiments with actin-binding drugs, synaptosomes were incubated with either latrunculin A (LAT A; Sigma-Aldrich) or jasplakinolide (JASP; Merck) for 1 h at 37 °C before further processing.

Glutamate release from forebrain synaptosomes was measured in an enzyme-linked fluorometric assay using the Fluoroskan ascent FL microplate reader (Labsystems) as described previously (Sim et al. 2006). Briefly, synaptosomes that were resuspended in Krebs buffer at a concentration of 1 mg/mL were incubated for 15 min at 37 °C in 2 mM $CaCl_2$, 2.5 mM $NADP^+$ (Applichem), and 15 U of glutamate dehydrogenase (Sigma-Aldrich). Glutamate release was induced by increasing the KCl concentration to 40 mM. Additionally, the fraction of Ca^{2+}-independent glutamate release was determined by measuring KCl-induced glutamate release after 60 min preincubation in Krebs-like buffer containing 1 mM EGTA, but no $CaCl_2$. The fraction of Ca^{2+}-independent glutamate release was subtracted from the depolarization-induced glutamate release. For calculating the ratio of late-to-early glutamate release, amounts of glutamate that were released between 100 and 430 s of KCl treatment were divided by those levels that were released within the first 10 s. The total synpatosomal glutamate content was determined after adding 0.1% Triton X-100 to lyse all synaptosomes.

vSNARE/tSNARE Ratio

Immunoprecipitation of syntaxin 1 for vSNARE/tSNARE ratio in hippocampal synaptosomes was essentially performed as described before (Pilo Boyl et al. 2007). Briefly, hippocampal synaptosomes (2 mg/mL) were lysed in lysis buffer [150 mM NaCl, 50 mM Tris, 1% Triton X-100, protease inhibitor (Roche); pH 7.5] and incubated overnight at 4 °C with a mouse anti-syntaxin 1 antibody (10 µg/200 µg sample). Syntaxin 1 antibody was precipitated with protein G sepharose beads (GE Healthcare) and separated from unbound sample in washing buffer (150 mM NaCl and 50 mM Tris; pH 7.4). Beads and the soluble fraction that were boiled in sample buffer (40 mM Tris, pH 6.8; 5% glycerol, 1% sodium dodecyl sulfate, and 2% β-mercaptoethanol) were separated by gel electrophoresis. The vSNARE/tSNARE ratios were calculated by western blot analysis of immunoprecipitated syntaxin 1 and bound synaptobrevin 2. Ratios of CTR samples were set to 1.

Antibodies for Biochemical Experiments

The following antibodies were used: mouse anti-actin (1 : 2000; MP Biochemicals), mouse anti-syntaxin 1 (1 : 1000, Synaptic Systems), and rabbit anti-synaptobrevin 2 (1 : 1000). Primary antibodies were detected using horseradish peroxidase-conjugated goat anti-mouse and goat anti-rabbit IgG-antibodies (1 : 5000; Thermo Fisher Scientific) and Western Lightning Plus chemiluminescence detection kit (Perkin-Elmer).

Electrophysiology

Tissue Preparation

Four- to 6-week-old mice were sacrificed by cervical dislocation and their brains were rapidly removed from the skulls and dissected in chilled solution (4 °C) containing (in mM): 87 NaCl, 2 KCl, 0.5 $CaCl_2$, 7 $MgCl_2$, 26 $NaHCO_3$, 1.25 NaH_2PO_4, 25 glucose, 75 sucrose, and bubbled with a mixture of 95% O_2/5% CO_2, leading to a pH of 7.4. About 300- to 370-µm-thick horizontal hippocampal slices were cut with a VT1200S vibratome (Leica), preincubated for 30 min at 37 °C, and then transferred to the recording solution containing (in mM): 125 NaCl, 2.5 KCl, 2 $CaCl_2$, 1.3 $MgSO_4$, 26 $NaHCO_3$, 1.25 NaH_2PO_4, 10 glucose, 2 sodium pyruvate, 3 myo-inositol, 0.44 ascorbic acid, and bubbled with a mixture of 95% O_2/5% CO_2. Slices rested in this recording solution for at least 1 h before recordings began.

Single-Cell Recordings

Patch pipettes had resistances of 4–8 MΩ when filled with a solution containing (in mM): 117.5 $CsMeSO_4$, 2.5 CsCl, 8 NaCl, 10 HEPES, 10 TEA, 0.2 EGTA, 4 Na_2ATP, 0.6 Na_2GTP, and 5 QX-314 (pH adjusted to 7.2 with CsOH). Slices were transferred to the recording chamber, which was continuously perfused at a rate of 1.5–2 mL/min with recording solution at room temperature (RT). CA1 hippocampal neurons were visualized with DIC-infrared optics using a ×60/1.0 water immersion objective on an upright Eclipe E600-FN microscope (Nikon). Electrophysiological responses were recorded with an EPC 10 patch-clamp amplifier and PatchMaster and the FitMaster software (HEKA Elektronik). For measurements of miniature excitatory postsynaptic currents (mEPSCs), the bath solution contained 4 mM $CaCl_2$ and 4 mM $MgSO_4$. During recordings, 0.5 µM tetrodotoxin (Tocris), 100 µM picrotoxin (Tocris), and 250 µM trichlormethiazide (Sigma-Aldrich) were applied via the bath. CA1 hippocampal neurons were voltage clamped at −70 mV, and spontaneous mEPSCs were recorded for 5 min. Amplitudes and inter-event intervals (IEIs) were analyzed with miniAnalysis (Synaptosoft), with an amplitude threshold of 3.5 pA.

Field Potential Recordings

For field potential experiments, pipettes were filled with 3 M NaCl, and field EPSPs (fEPSPs) were measured at a stimulus intensity that elicited amplitudes that were approximately 30–50% of the maximum. Input–output curves were built by measuring the fiber volley (FV) and fEPSP of the responses evoked by stimulating afferent fibers with current intensities ranging from 20 to 300 µA. Paired-pulse ratio (PPR) was analyzed by applying pairs of stimuli at the following ISI (in ms): 10, 15,

25, 50, 75, and 100. Short-term depression was monitored during stimulation at 10 Hz for 2 full minutes in the presence of D-(-)-2-Amino-5-phosphonopentanoic acid.

Synapse Morphology

Golgi Staining

Mice at P40–P42 were used for Golgi-Cox staining exploiting the FD Rapid GolgiStain™ kit (FD Neurotechnologies). Tissue impregnation and tissue section staining were performed according to the manufacturer's data sheet. Briefly, mice were perfused intracranially with 4% formaldehyde and brains were removed from the skull and postfixed in 4% formaldehyde overnight. After incubation in impregnation solution and solution C, brains were imbedded in gelatin–albumin and cut into 100 µm coronal sections using a vibrating microtome (Campden Instruments, Ltd.). Sections were mounted onto gelatinized glass slides, further processed for Golgi staining procedure, and finally mounted in Entellan (Merck). High magnification images of second-order dendritic branches in the hippocampal CA1 *stratum radiatum* were generated by using an Axioskop microscope and a Plan-Neofluar ×100/1.30 oil immersion objective (Carl Zeiss). Image acquisition and measurement of spine density were performed by an experimenter blind to the genotype of the mice.

Electron Microscopy

Young adult (P40–P42) mice were perfused with 1% formaldehyde/1% glutaraldehyde in phosphate buffer (0.1 M PB, pH 7.4). The brains were postfixed in the same fixative overnight, and small specimens taken from the dorsal hippocampus were postfixed in 1% OsO_4 in 0.1 M cacodylate buffer, dehydrated, and embedded in epoxy resin. Ultrathin sections were stained with uranyl acetate and lead citrate and observed in a JEM-1010 transmission electron microscope (EM; Jeol) equipped with a side-mounted CCD camera (Mega View III, Soft Imaging System). Spine density was assessed by analyzing 140 digitized images from 3 mice of each group. Images (×30 000 magnification and size 14.66 μm^2) were captured in the proximal part of CA1 *stratum radiatum*. Morphometric analysis was done on electron micrographs taken at ×75 000 using the ImageJ 1.52q imaging software (NIH). Synaptic structures were identified by presynaptic terminals with at least 3 synaptic vesicles, a visible synaptic cleft and a well-defined postsynaptic density (PSD). Vesicles contacting the active zone were considered as physically docked vesicles. Image acquisition and morphometric analysis were performed by an experimenter blind to the genotype of the mice.

Histology

Young adult mice (P38–P40) were perfused with 4% paraformaldehyde (PFA). Brains were postfixed in the same fixative for 6 h and then transferred overnight into 30% sucrose/PBS for cryo-protection. Fifty-µm-thick coronal sections were cut on a HM 400R sliding microtome (Microm) and collected in 15% sucrose/PBS.

X-Gal Staining

Sections were fixed for 10 min in a PBS-based fixation solution containing 0.1% sodium desoxycholate, 0.2% NP-40, 1% PFA, and 0.2% glutaraldehyde. Thereafter, sections were stained at 30 °C for at least 2 h in a PBS-based staining solution containing 2 mM $MgCl_2$, 5 mM $K_3Fe(CN)_6$, 5 mM $K_4Fe(CN)_6$, 0.1% sodium deoxycholate, 0.2% NP-40, and 1 mg/mL X-Gal in PBS. After washing, sections were mounted on glass slides, counterstained with Fast Red (Vector Laboratories), dehydrated in alcohol and xylene, and embedded in Entellan (Merck). Images were generated using an Axioskop2 microscope (Zeiss), a DP20 CCD camera system, and Cell^P software (Olympus).

Immunohistochemistry

After a 30-min incubation step in 10 mM citrate buffer, sections were blocked for 1 h at RT in PBS containing 0.3% Triton X-100 (Roth), 2% bovine serum albumin (AppliChem), and 10% normal goat serum (Invitrogen). Thereafter, sections were incubated overnight at 4 °C with primary antibodies [rabbit anti-β-galactosidase (1 : 2000, MP Biomedicals) and mouse anti-NeuN (1 : 1000, Millipore)] diluted in blocking solution. After an additional 30-min blocking step, sections were incubated for 1 h with secondary antibodies (Alexa Fluor 488-conjugated goat anti-mouse or Alexa Fluor 647-conjugated goat anti-rabbit, 1 : 1000; Invitrogen) in blocking solution. After washing, sections were mounted in home-made mounting medium (Herde et al. 2010). Low magnification micrographs were taken with a Zeiss Axioskop2 microscope equipped with F-view 2 camera system and Cell^P software (Olympus). High magnification micrographs were acquired with an LSM 510 confocal microscope (Zeiss) equipped with Apochromat ×20/0.8 and ×40/1.3 objectives. Pinhole settings were adjusted to achieve optical sections of 10 µm thickness. Images were further processed with the LSM Image browser software 4.20 (Zeiss) and Image J 1.42s (NIH).

Statistical Analysis

Sets of data are presented by their mean values and standard error of the means (SEMs). For some experiments, the median and the 25% and 75% values are given in addition to the mean value and SEM. An unpaired two-tailed Student's *t*-test was used when comparing 2 sets of data with normal distribution.

Results

Inactivation of n-Cofilin in the Hippocampus

To test for overlapping synaptic functions of ADF and n-cofilin and to clarify the general relevance of ADF/cofilin for presynaptic physiology, we generated double-mutant mice (termed ACC mice) that lack ADF systemically and n-cofilin specifically in principal neurons of the adult forebrain (Bellenchi et al. 2007; Rust et al. 2010). Forebrain-specific inactivation of n-cofilin was achieved by crossing conditional n-cofilin mutants to transgenic mice that express cre recombinase under control of the CaMKIIα subunit (Minichiello et al. 1999). By exploiting Rosa 26 cre reporter mice, efficient cre activation was evident in all hippocampal regions of P38–P40 CaMKII-cre mice (Fig. 1*A*). Co-immunolabeling for β-galactosidase and the neuronal marker NeuN revealed active cre in >95% of the neurons in the hippocampal CA3 and CA1 regions (Fig. 1*B–E*; CA3: 95.1 ± 0.6%; CA1: 97.6 ± 0.8%; 6 images from 3 mice). Hence, hippocampal CA3–CA1 synapses of ACC mice are suitable for investigating synaptic functions of ADF and n-cofilin.

Synaptic Actin Dynamics Depend on ADF/Cofilin

We next examined synaptic actin dynamics in ACC mice by exploiting synaptosomal preparations and by calculating the ratio of F-actin to monomeric actin (G-actin). We previously showed that genetic inactivation of n-cofilin caused similar changes in the F/G-actin ratios in cortical and hippocampal synaptosomes (Rust et al. 2010). To increase synaptosomal yield, we here decided to exploit synaptosomes isolated from forebrain tissues that mainly contained cerebral cortex and hippocampus, but also striatum. The presence of ADF and n-cofilin in forebrain synaptosomes has been reported before (Rust et al. 2010; Görlich et al. 2011). The soluble cytoskeletal fraction (including G-actin) was separated from the insoluble fraction (containing F-actin) and actin levels were quantified (Fig. 2*A*). While the synaptic F/G-actin ratio was unchanged in ADF mutants compared with CTR, increased ratios were observed in n-cofilin mutants and ACC mice (Fig. 2*B*; CTR: 1.01 ± 0.08, $n = 8$ preparations from 8 mice; ADF: 1.20 ± 0.04, $n = 8/8$, $P = 0.064$; n-cofilin: 1.54 ± 0.06, $n = 8/8$, $P < 0.001$;

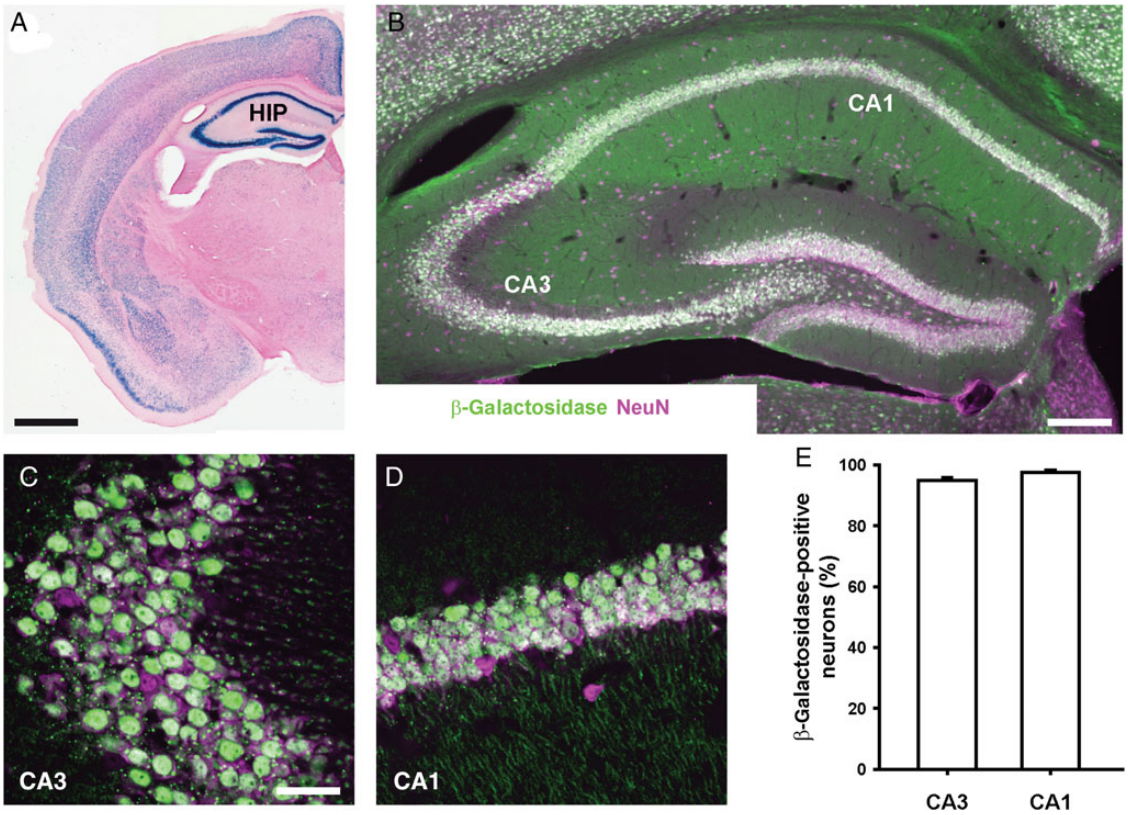

Figure 1. Cre activity in the hippocampus. (*A*) β-Galactosidase staining of P38–P40 Rosa26 cre reporter/CaMKII-cre transgenic mice revealed very efficient cre activity in the entire hippocampus (HIP). Scale bar: 500 μm. (*B*) In hippocampal CA1 and CA3 regions of these mice, the majority of neurons identified by NeuN immunoreactivity (magenta) were positive for β-galactosidase (green). Scale bar: 250 μm. (*C* and *D*) β-Galactosidase and NeuN immunolabeling in the hippocampal CA3 and CA1 regions at high magnification. Scale bar in *C* 50 μm, also for *D*. (*E*) Percentage of β-galactosidase-positive neurons in the CA3 and CA1 stratum pyramidale.

ACC: 2.33 ± 0.16, $n = 7/7$, $P < 0.001$). Notably, in ACC mice, the increase of the synaptic F/G-actin ratio was higher than in n-cofilin mutants ($P < 0.001$), showing the synergistic activity of ADF and n-cofilin. Similar results were obtained when analyzing hippocampal synaptosomes (data not shown).

Depolarization of synaptosomes induces cycling of actin assembly and disassembly (Bernstein and Bamburg 1989; Yamada et al. 2009) and strongly increases the F/G-actin ratio (Pilo Boyl et al. 2007). To test whether ADF/cofilin controls stimulated actin dynamics, we depolarized forebrain synaptosomes for various durations (0–60 s) with 40 mM extra-synaptosomal KCl. In CTR synaptosomes, KCl treatment induced oscillations of actin polymerization including actin assembly after 3 s (Fig. 2*C*, *D*) that was followed by actin disassembly after 10 s and a further increase of the F/G-actin ratio, similar to previous results (Bernstein and Bamburg 1989; Yamada et al. 2009). While inactivation of ADF did not impair activity-dependent F-actin oscillation, such kinetics of actin assembly/disassembly was absent from n-cofilin mutants and ACC mutants (Fig. 2*D*, arrow). Compared with n-cofilin mutants, the synaptic F/G-actin ratio was increased in ACC mice at all time-points examined. Notably, an increase of 22% in the F/G-actin ratio upon KCl treatment indicates that d*e novo* actin polymerization could still occur in ACC synaptosomes (0 s: 2.33 ± 0.16, $n = 7$ preparations from 7 mice, 60 s: 2.85 ± 0.13, $n = 6/6$, $P < 0.05$). However, it was markedly reduced when compared with CTR in which KCl treatment increased the F/G-actin ratio by 67% (0 s: 1.01 ± 0.08, $n = 8/8$, 60 s: 1.69 ± 0.09, $n = 6/6$, $P < 0.001$). Taken together, these data show that, in the absence of ADF and n-cofilin, *de novo* actin polymerization is inducible in synapses. However, ADF/cofilin is essential for stimulated actin remodeling, which is known to occur during vesicle release.

The increased synaptic F/G-actin ratios and the lack of the disassembly phase in depolarized ACC synaptosomes are in agreement with actin-depolymerizing activity of ADF and n-cofilin. Impaired synaptic actin depolymerization in ACC mice was further supported by experiments using LAT A, which sequesters G-actin and, in the presence of actin-depolymerizing activity, facilitates breakdown of F-actin (Spector et al. 1989). In forebrain synaptosomes from control mice, LAT A decreased the F/G-actin ratio in a dose-dependent manner (Fig. 2*E*,*F*; 0 μM: 0.95 ± 0.04; 0.2 μM: 0.72 ± 0.05, $P < 0.05$; 2 μM: 0.60 ± 0.05, $P < 0.001$; $n = 5$ preparations from 3 mice). Conversely, LAT A did not affect the F/G-actin ratio in ACC synaptosomes (0 μM: 2.00 ± 0.18; 0.2 μM: 2.01 ± 0.08, $P = 0.959$; 2 μM: 1.85 ± 0.08, $P = 0.485$; $n = 5/3$). Furthermore, the F-actin stabilizing drug JASP (Tsuji et al. 2009) increased the F/G-actin ratio in forebrain synaptosomes from control mice by 128% (Fig. 2*G*,*H*; 0 μM: 1.11 ± 0.12; 20 μM: 2.53 ± 0.26, $P < 0.01$; $n = 5/3$), but only small changes were seen in ACC synaptosomes (0 μM: 2.18 ± 0.26; 20 μM: 3.19 ± 0.27, +46%, $n = 4/3$, $P < 0.05$). These data suggest that it is the actin-depolymerizing activity of ADF/cofilin that is critical for synaptic actin remodeling.

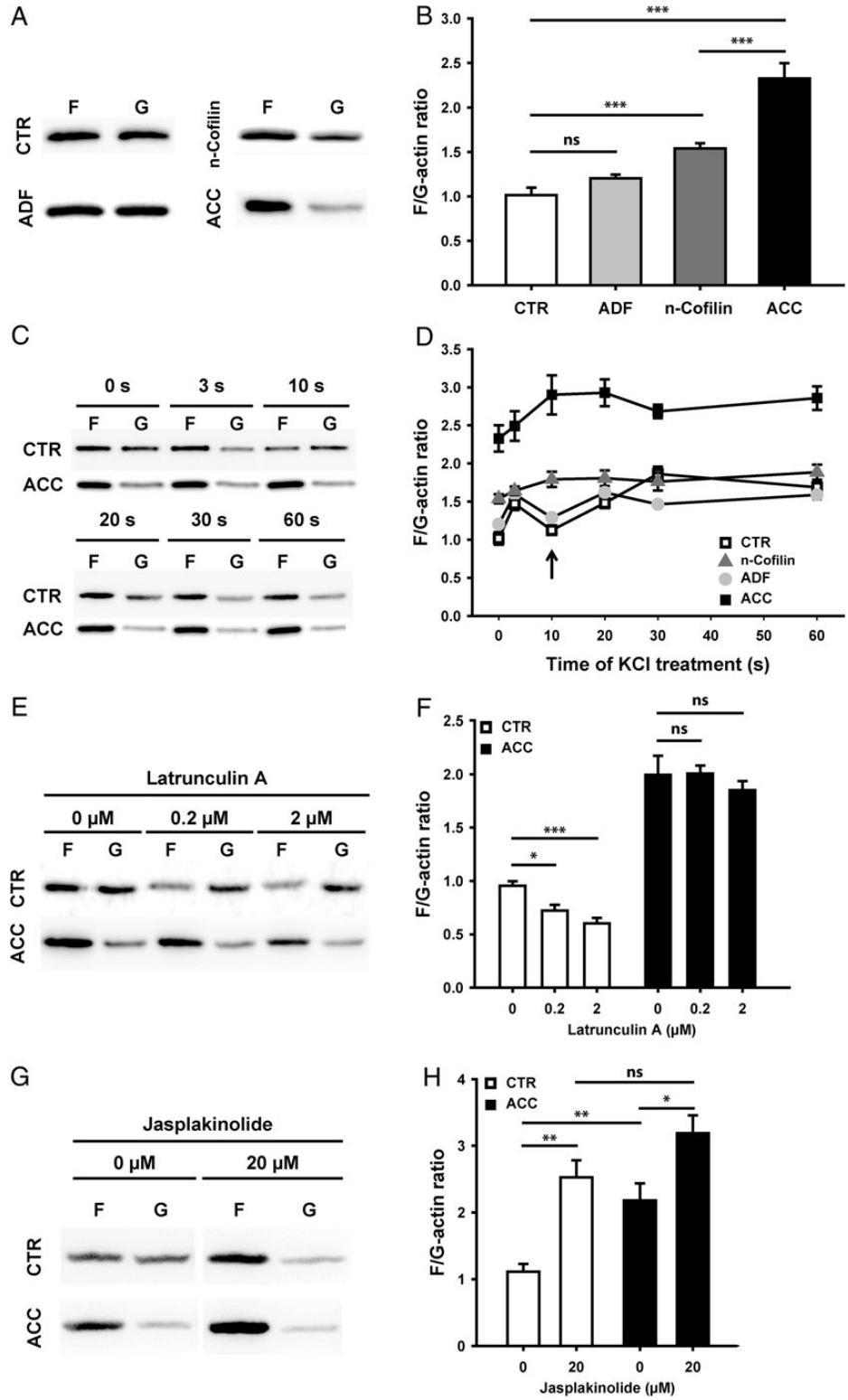

Figure 2. Impaired synaptic actin dynamics in ACC mice. (*A*) Immunoblots showing actin levels in the insoluble (F) and the soluble protein fraction (G) of synaptosomes of forebrain tissue (cerebral cortex, hippocampus, and striatum) from a control mouse (CTR), an ADF mutant (ADF), a n-cofilin mutant (n-cofilin), and a double mutant (ACC). (*B*) In ADF mutants, the F/G-actin ratio was unchanged, while it was increased in n-cofilin mutants and ACC mice. (*C*) Immunoblots from a CTR and an ACC mouse, showing changes in synaptosomal F- and G-actin levels upon KCl-induced depolarization. (*D*) Depolarization of forebrain synaptosomes induced cyclic actin assembly and disassembly in CTR and ADF mutants, but not in n-cofilin mutants and ACC mice. Notably, actin disassembly was present in CTR and ADF mutants, but not in n-cofilin mutants and ACC mice (arrow). (*E*) Immunoblots showing actin in insoluble and soluble protein fractions upon treatment with LAT A. (*F*) LAT A reduced F/G-actin ratio in CTR, but not in ACC mice. (*G*) Immunoblots showing actin in insoluble and soluble protein fractions upon treatment with 20 μM JASP. (*H*) JASP increased F/G-actin ratios in CTR and ACC mice. However, the increase was smaller in ACC mice, and after JASP treatment, the F/G-actin ratios did not differ between both groups. F: actin in the insoluble protein fraction; G: actin in the soluble protein fraction; ns: not significant; $^{*}P < 0.05$; $^{**}P < 0.01$; $^{***}P < 0.001$.

Enlarged Dendritic Spines and Reduced Synapse Density in ACC Mice

The impairment in synaptic actin dynamics prompted us to investigate synapse morphology in ACC mice. We first performed an EM analysis in the hippocampal CA1 *stratum radiatum* at postnatal day 40 (P40) (Fig. 3*A*,*B*). Spine profiles were unusually large in ACC mice, and quantitative analyses revealed a 77% increase over the control situation (Fig. 3*C*; CTR: 0.098 ± 0.004 µm^2, $n = 181$ spines from 3 mice; ACC: 0.173 ± 0.009, $n = 164/3$, $P < 0.001$). By comparison, in n-cofilin mutants, spine size was enlarged by only 26% compared with CTR (0.123 ± 0.006, $n = 170/3$, $P < 0.001$). The difference between n-cofilin mutants and ACC mice was also significant ($P < 0.001$), indicative of a relevance of ADF in dendritic spines.

Interestingly, spine enlargement was accompanied by a 39% decrease in the density of axo-spinous synapses in ACC mice (Fig. 3*D*; CTR: 0.56 ± 0.02 synapses/µm^2, total analyzed area in 3 mice: 2125.7 µm^2; ACC: 0.34 ± 0.01 synapses/µm^2, 2052.4 µm^2/3 mice; $P < 0.001$). The reduction in synapse density was confirmed by the analysis of Golgi-stained CA1 pyramidal cells (Fig. 3*E*). Compared with CTR, the density of spines along dendritic profiles was reduced by 26% in ACC mice (Fig. 3*F*; CTR: 26.6 ± 0.9 spines/20 µm dendrite, $n = 33$ dendritic shafts from 3 mice; ACC: 19.8 ± 0.8 spines/20 µm dendrite, $n = 31/3$, $P < 0.001$).

Impaired Organization of Synaptic Vesicles in ACC Mice

The synaptic vesicle organization in presynaptic terminals depends on the actin cytoskeleton (Dillon and Goda 2005; Cingolani and Goda 2008). By exploiting EM micrographs of the CA1 *stratum radiatum*, we studied the distribution of vesicles in mutant mice and determined their distances to the active zone. In ACC mice, the relative number of synaptic vesicles was reduced within a region close to the active zone (Fig. 4*A*; ≤100 nm; CTR: $58.0 \pm 3.0\%$, $n = 53$ presynaptic terminals from 3 mice; ACC: $41.5 \pm 2.3\%$, $n = 53/3$; $P < 0.001$), whereas it was increased in a region >250 nm away from the active zone (CTR: $11.4 \pm 1.4\%$; ACC: $19.9 \pm 1.5\%$; $P < 0.001$). Conversely, the relative vesicle numbers were unchanged in ADF (≤100 nm: $55.4 \pm 2.6\%$, $P = 0.581$; 250–350 nm: $13.9 \pm 1.9\%$, $P = 0.292$; $n = 56/3$) or n-cofilin mutants (≤100 nm: $53.9 \pm 3.2\%$, $P = 0.356$; $12.7 \pm 1.7\%$, $P = 0.578$; $n = 45/3$). In addition to the altered vesicle distribution, we noted a 24% increase in the number of docked vesicles in ACC mice (Fig. 4*B*; CTR: 11.3 ± 0.8 vesicles/µm of PSD, $n = 70$ active zones from 3 mice; ACC: 14.0 ± 0.8 vesicles/µm PSD, +24%, $n = 70/3$, $P < 0.05$). No such change was found in n-cofilin (11.9 ± 0.9 vesicles/µm PSD, $n = 62/3$; $P = 0.631$) or ADF single mutants (Görlich et al. 2011). To further test whether the number of fusion-compatible, primed vesicles was increased in ACC mice, we quantified the fraction of the vSNARE synaptobrevin 2 bound to the tSNARE syntaxin 1 in a co-immunoprecipitation approach by exploiting hippocampal synaptosomes (Murthy and De Camilli 2003; Pilo Boyl et al. 2007). Compared with CTR, we found a 67% increase of complexed synaptobrevin 2 in ACC synaptosomes (Fig. 4*C*; CTR: 1.00 ± 0.14; ACC: 1.67 ± 0.26; $n = 5$ preparations from 5 mice for both groups; $P < 0.05$). In summary, EM studies and biochemical data in ACC mutants showed a shift in vesicle distribution from the active zone to the reserve pool, accompanied by an increased docking of vesicles at the plasma membrane.

Impaired Vesicle Recruitment in ACC Mice

The altered vesicle distribution in ACC mutants suggested that ADF/cofilin is crucial for synaptic vesicle organization. One would expect that these changes might also affect neurotransmitter release. To test this hypothesis, we isolated forebrain synaptosomes and quantified depolarization-induced glutamate release by performing an enzyme-linked fluorometric assay (Nicholls et al. 1987). In agreement with the normal vesicle distribution in ADF and n-cofilin mutants, the depolarization of synaptosomes with 40 mM KCl did not change glutamate release in the respective single mutants (Fig. 5*A*,*B*; CTR: 5.35 ± 0.18 nmol/mg protein, $n = 21$ preparations from 11 mice; ADF: 5.33 ± 0.12 nmol/mg protein, $n = 8/4$, $P = 0.942$; n-cofilin: 5.42 ± 0.47 nmol/mg protein, $n = 8/4$, $P = 0.880$). However, glutamate release was decreased in ACC synaptosomes and reached only 76% of CTR values (4.09 ± 0.12 nmol/mg protein, $n = 21/11$, $P < 0.001$). Quantification of total glutamate contents showed comparable levels in ADF mutants, n-cofilin mutants, and CTR (Fig. 5*C*; CTR: 21.97 ± 0.48 nmol/mg protein, $n = 22/11$; ADF: 22.94 ± 0.61 nmol/mg protein, $n = 12/4$, $P = 0.239$; n-cofilin: 23.59 ± 0.72 nmol/mg protein, $n = 11/6$, $P = 0.061$). In contrast, ACC mutants showed an increased glutamate content (27.14 ± 0.57 nmol/mg protein, $n = 15/6$, $P < 0.001$). Hence, the decreased glutamate release in ACC mutants is not caused by overall reduced glutamate levels. Interestingly, the early phase of glutamate release (during the first 10 s of KCl treatment) was unchanged in ACC mice, and only the late phase was altered (100–430 s). Accordingly, the ratio of late-to-early glutamate release was reduced in ACC synaptosomes (Fig. 5*D*; CTR: 1.89 ± 0.08; ACC: 1.28 ± 0.09; $P < 0.001$). Such a defect is in agreement with defective vesicle recruitment to the release sites. To test whether vesicle recruitment was indeed impaired in ACC mice, we performed a short-term depression protocol on acute hippocampal slices (10 Hz stimulation of Schaffer collaterals for 2 min), to deplete the readily releasable pool of presynaptic vesicles in CA3–CA1 synapses. The amplitudes of the recorded excitatory postsynaptic field potentials (fEPSP) rapidly declined in CTR and ACC slices (Fig. 5*E*). However, the baseline between minute 3.5 and 4 of the recording was reduced by 59% in ACC mice, which indicates a defect in vesicle recruitment (inset; last 30 s: CTR: 0.154 ± 0.018, $n = 13$ slices from 4 mice; ACC: 0.064 ± 0.016, $n = 12/4$; $P < 0.01$). When comparing the first 25 stimuli of the recordings, this stimulation resulted in a typical potentiation in CTR, but not in ACC slices. Beginning with the third stimulus of the 10-Hz train, the fEPSP slope was significantly lower in ACC slices when compared with CTR (Fig. 5*F*), indicative of an increased vesicle release in ACC mice. Notably, such changes were not detectable in ADF and n-cofilin single mutants (Rust et al. 2010; Görlich et al. 2011). The faster depletion in ACC mutants is in agreement with the observed increased number of docked vesicles and the concomitant depletion of vesicles in the vicinity of the plasma membrane.

ADF/Cofilin Is Involved in Synaptic Vesicle Exocytosis

The elevated number of docked vesicles in ACC mice and the increased vSNARE/tSNARE ratio suggested an increased rate of vesicle exocytosis in ACC mice. To test this hypothesis, we recorded mEPSCs from individual CA1 pyramidal cells of acute hippocampal slices (Fig. 6*A*). In ACC mice, both the amplitudes (Fig. 6*B*; CTR: 7.57 ± 0.32 pA; ACC: 7.04 ± 0.23 pA; $n = 20$

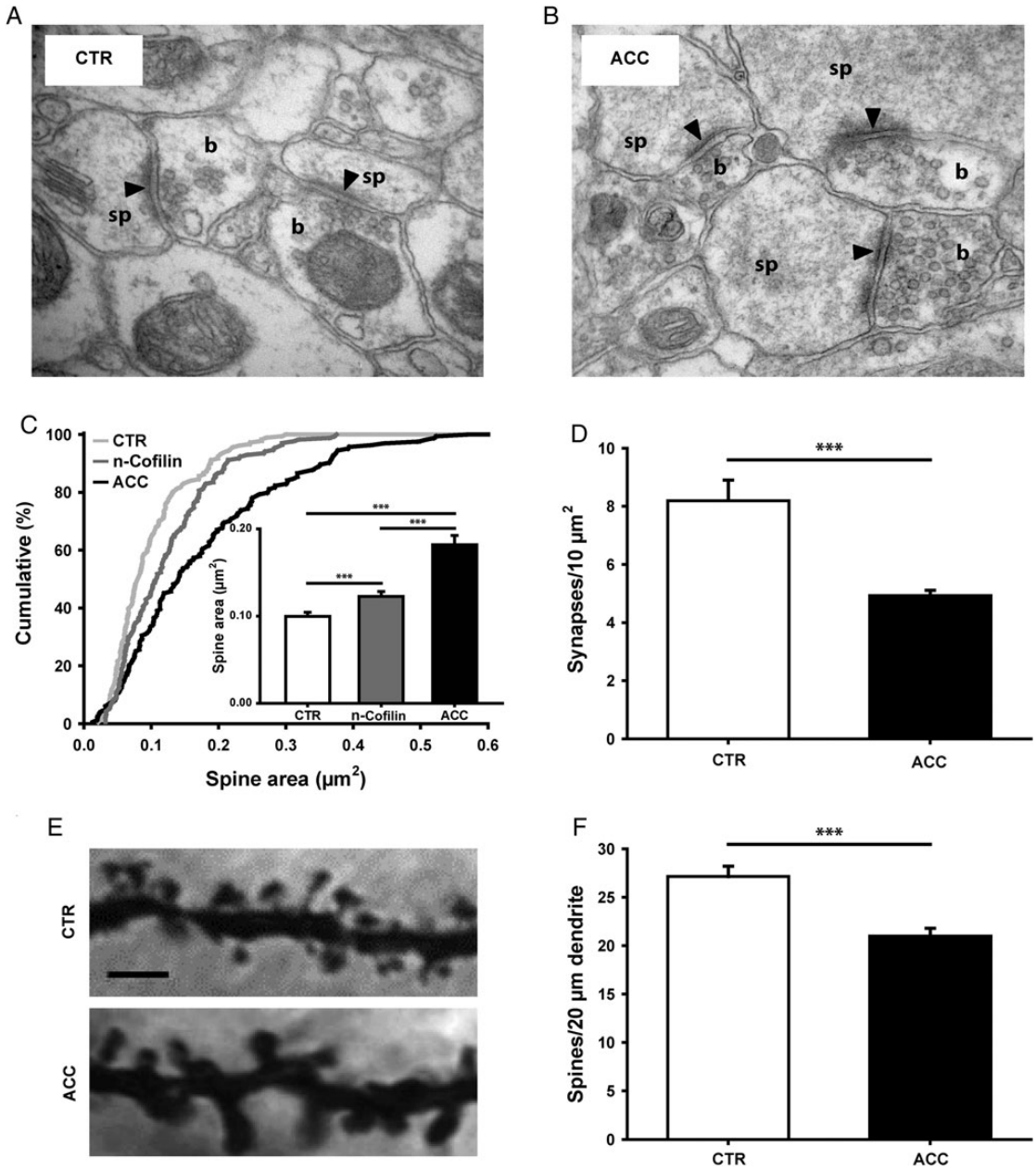

Figure 3. Enlarged dendritic spines and reduced synapse density in ACC mice. (*A* and *B*) Electron micrographs of the CA1 *stratum radiatum* from a CTR and an ACC mouse. Image size: 2.27 μm^2; b: presynaptic bouton; sp: postsynaptic spine; arrowhead: PSD. (*C*) Cumulative curve and mean values showing increased spine size in n-cofilin mutants. Compared with n-cofilin mutants, spine size was further increased in ACC mice. (*D*) Reduced density of excitatory synapses in CA1 *stratum radiatum* of ACC mice. (*E*) Images showing second-order dendritic branches from Golgi-stained pyramidal cells in the CA1 *stratum radiatum*. Scale bar: 2.5 μm. (*F*) In ACC mice, the spine density along dendritic profiles was reduced. $^{***}P < 0.001$.

cells from 7 mice for both groups; $P = 0.187$) and the IEI were unchanged (Fig. 6*C*; CTR: 0.79 ± 0.04 s; ACC: 0.73 ± 0.05 s; $n = 20$ cells from 7 mice for both groups; $P = 0.347$). This was a surprising result, since the IEI directly depends on vesicle release probability and the number of excitatory synapses (El-Husseini et al. 2000). One explanation would be that the decreased synapse density in ACC mice (Fig. 3*D*,*F*) might obscure a change in release probability. We therefore stimulated Schaffer collaterals with various stimulus intensities (20–300 µA) and recorded field potentials in the CA1 *stratum radiatum*. Consistent with the reduced synapse density, we found reduced FV amplitudes in ACC mice upon stimulation with intensities >40 µA (Fig. 6*D*; e.g. 100 µA: CTR: 1.15 ± 0.09 mV, $n = 15$ slices from 4 mice; ACC: 0.75 ± 0.08 mV, $n = 14/3$; −35%; $P < 0.001$). Conversely, at none of the stimulus intensities examined did we find differences in the fEPSP slopes between CTR and ACC mice (Fig. 6*E*; e.g. 100 µA: CTR: 2.37 ± 0.34 mV/ms; ACC: 2.48 ± 0.26 mV/ms; $P = 0.797$). Consequently, the resulting input–output curve showed a steeper rise in ACC mice (Fig. 6*F*), which is also indicated by higher fEPSP slope-to-FV amplitude ratios for stimulation intensities ≥60 µA (Fig. 6*G*). Since the normal mEPSC amplitudes exclude an altered transmitter load of synaptic vesicles in ACC mice, the unchanged fEPSP slopes upon stimulation of a reduced

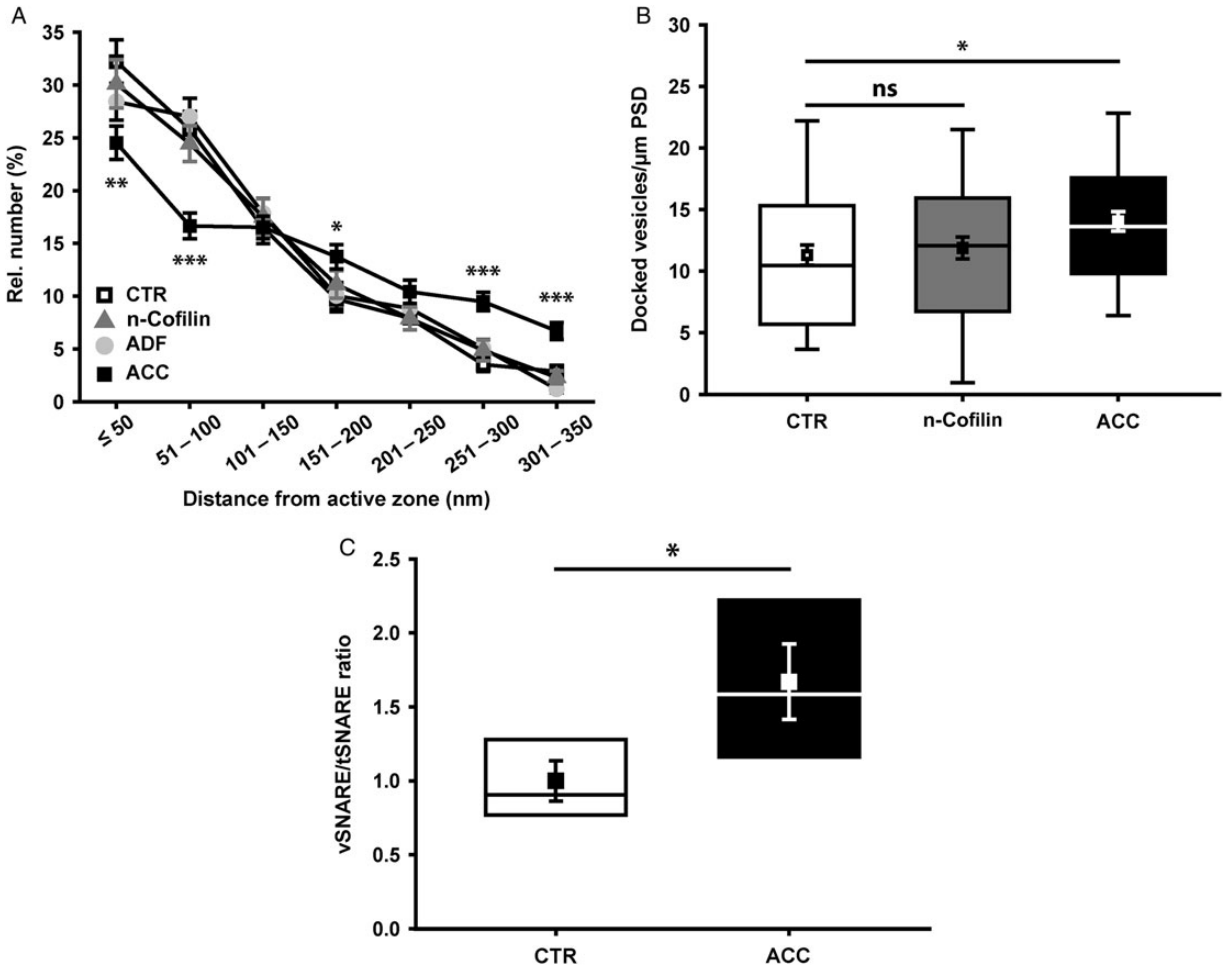

Figure 4. Altered organization of synaptic vesicles in ACC mice. (*A*) In ACC mice, the distribution of synaptic vesicles was altered, whereas it was normal in ADF or n-cofilin single mutants. Within a distance of 100 nm from the active zone, the relative number of synaptic vesicles was reduced in ACC mice, whereas it was increased between 250 and 350 nm away from the active zone. (*B*) In ACC mice, yet not in n-cofilin mutants, the number of docked vesicles was increased. (*C*) In a biochemical assay, more synaptobrevin 2 (vSNARE) was bound to the tSNARE syntaxin 1 in hippocampal synaptosomes from ACC mice when compared with CTR synaptosomes. ns: not significant; $^{*}P < 0.05$; $^{**}P < 0.01$; $^{***}P < 0.001$.

number of synapses are likely the result of an increased number of exocytosed vesicles. To test this, we measured the PPR at various inter-stimulus intervals (ISI), ranging from 10 to 100 ms. Indeed, in ACC mice, the PPR was reduced at 10 ms (Fig. 6*H*; CTR: 0.99 ± 0.04, $n = 15$ slices from 9 mice; ACC: 0.81 ± 0.04, $n = 14/5$; $P < 0.01$) and 15 ms (CTR: 1.10 ± 0.03; ACC: 0.96 ± 0.04; $P < 0.01$). No such changes were found in ADF or n-cofilin single mutants (Rust et al. 2010; Görlich et al. 2011). Taken together, our data reveal a novel function of ADF/cofilin in presynaptic physiology as they demonstrate that ADF/cofilin is involved in regulating vesicle distribution and exocytosis.

Discussion

In this study, we show impaired synaptic actin dynamics in ACC mice lacking the actin-depolymerizing proteins ADF and n-cofilin. In these mice, defects in synaptic actin dynamics cause impaired synaptic vesicle organization, mobilization, and exocytosis. Notably, these defects have not been observed in ADF or n-cofilin single mutants (Rust et al. 2010; Görlich et al. 2011). Hence, we demonstrate for the first time that ADF/cofilin-mediated actin dynamics is critical for presynaptic physiology. Moreover, we conclude that, besides n-cofilin, ADF is also important for excitatory synapses. Taken together with our previous analyses of single mutants, we conclude that ADF and n-cofilin have the capacity to compensate for the other's inactivation *in vivo*—findings that have not been reported before. Finally, our data suggest that a "dynamic actin cycle" is essential for controlled vesicle exocytosis and neurotransmitter release.

The role of n-cofilin in excitatory synapses has been extensively studied and its importance for postsynaptic plasticity and behavior has been highlighted by a number of publications (Fukazawa et al. 2003; Zhou et al. 2004; Hotulainen et al. 2009; Gu et al. 2010; Rust et al. 2010; Goodson et al. 2012; Wang et al. 2013). Conversely, the synaptic function of its close homologue ADF has remained obscure. ADF is located at pre- and postsynaptic structures of excitatory synapses, but ADF mutants display no synaptic defects (Görlich et al. 2011). In agreement with a predominant role of n-cofilin in excitatory synapses, we found impaired synaptic actin dynamics in mutants for n-cofilin, but not for ADF. Interestingly, defects in synaptic actin dynamics were stronger in ACC mice,

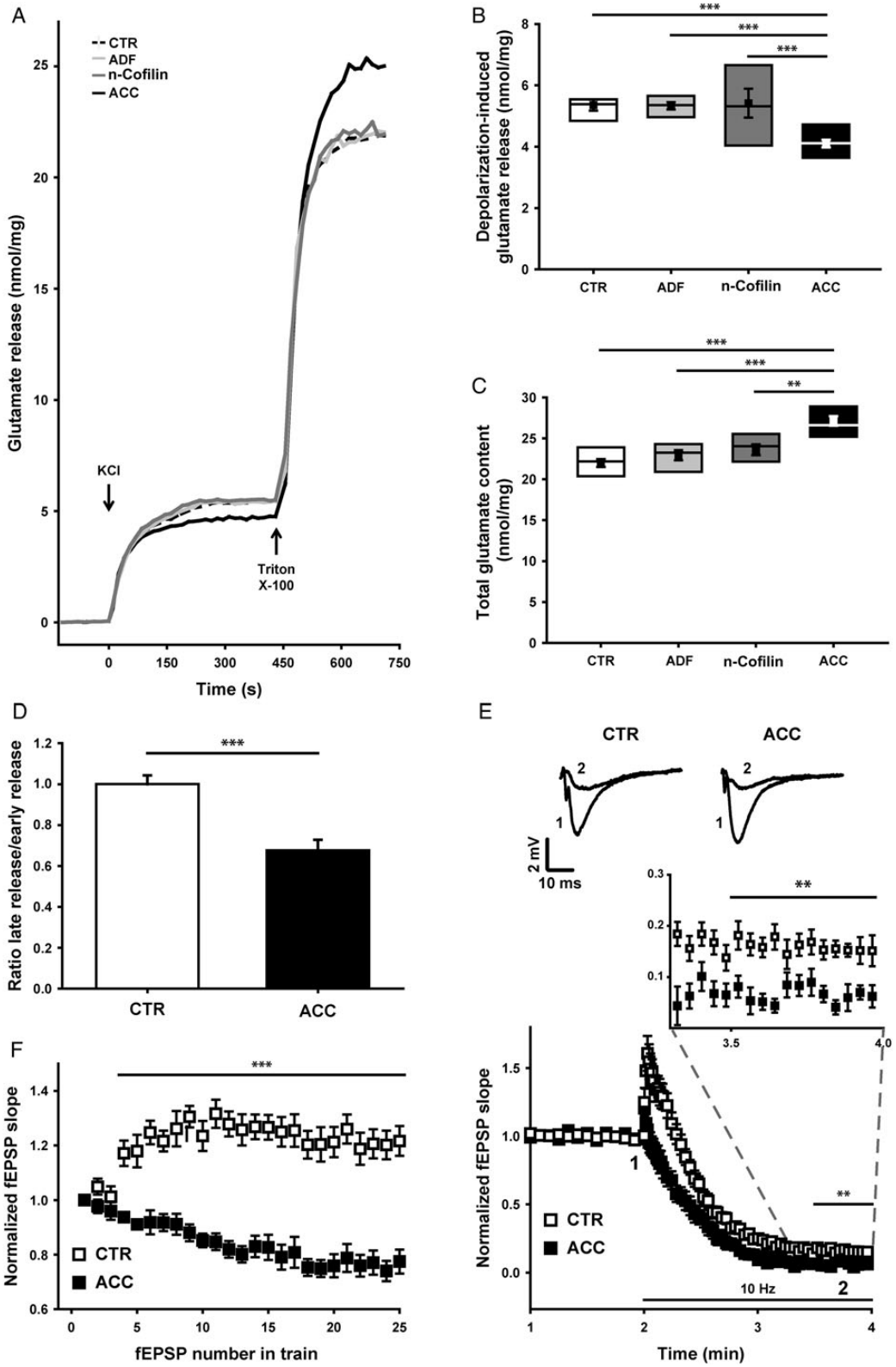

Figure 5. Impaired glutamate release from ACC synaptosomes. (*A*) Representative traces showing KCl-induced glutamate release from forebrain synaptosomes and total glutamate content that was determined after Triton X-100 lysis. (*B*) In ACC mice, but not in ADF or n-cofilin single mutants, depolarization-induced glutamate release was reduced. (*C*) Triton X-100 was used to lyse forebrain synaptosomes and to determine the total glutamate content. It was significantly increased in ACC mice, but not in single mutants. (*D*) The ratio of late (100–430 s) to early (0–10 s) glutamate release was reduced in forebrain synaptosomes from ACC mice compared with CTR synaptosomes. (*E*) Upper part: Exemplary fEPSP traces from a CTR and an ACC mouse (1) before and (2) 135 s after the beginning of Schaffer collateral stimulation with 10 Hz. Lower part: Short-term depression, induced by stimulation of Schaffer collaterals for 2 min with 10 Hz in the presence of the NMDA receptor agonist APV, resulted in a reduced fEPSP baseline in ACC mice between 3.5 and 4 min. Inset shows the last 40 s of the recordings at higher magnification. (*F*) A 10-Hz stimulation induced a potentiation in the fEPSP slope in CTR, but not in ACC slices. Note, in contrast to panel *E* of this figure, fEPSP slopes were normalized to the first response of the 10-Hz stimulation. $^{**}P < 0.01$; $^{***}P < 0.001$.

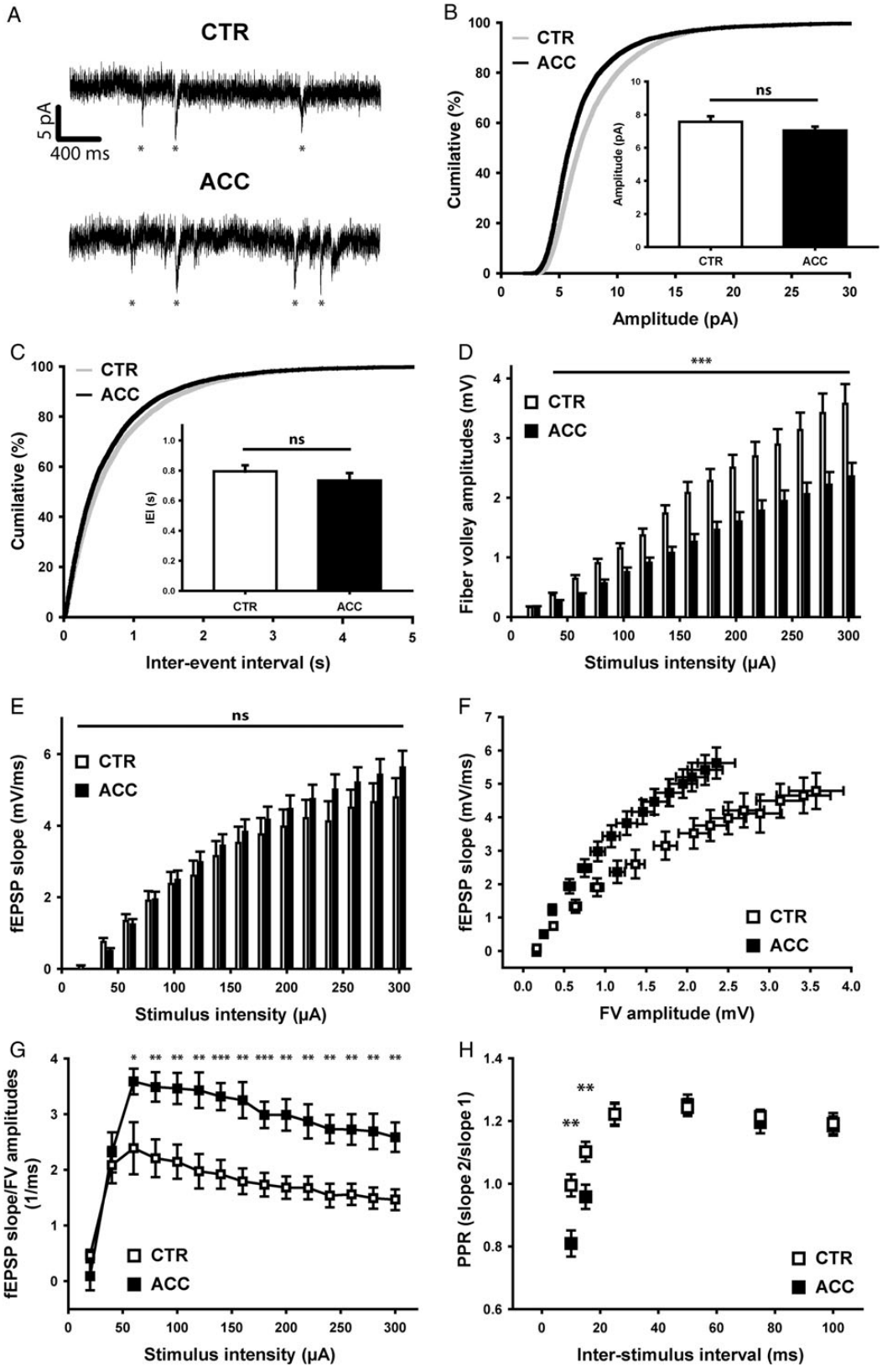

Figure 6. Impaired vesicle exocytosis in ACC mice. (*A*) Exemplary traces of mEPSCs from a CTR and an ACC mouse. Asterisks indicate events included into the analyses. (*B*) Amplitudes and (*C*) IEIs of mEPSCs recorded from CA1 pyramidal cells were unchanged in ACC mice. (*D*) Presynaptic FV amplitudes and (*E*) extracellulary recorded postsynaptic responses (fEPSP slope) to Schaffer collateral stimulation (intensities ranging from 20 to 300 μA) as measured in the hippocampal CA1 region. In ACC mice, FV amplitudes were reduced at stimulus intensities from 40 to 300 μA. Conversely, fEPSP slopes did not differ between CTR and ACC mice. (*F*) Input–output curve shows a steeper rise in ACC mice. (*G*) Compared with controls, the ratio of fEPSP slopes to FV amplitudes is increased in ACC mice at stimulus intensities $\geq$60 μA. (*H*) PPR was reduced in ACC mice at ISIs of 10 and 15 ms, but not at longer intervals (25–100 ms). ns: not significant; $^{*}P < 0.05$; $^{**}P < 0.01$; $^{***}P < 0.001$.

and these mutants showed impairments in synapse physiology (mobilization and exocytosis of vesicles, glutamate release) that were not present in n-cofilin mutants (Rust et al. 2010). Hence, ADF is also an important player in synapse physiology. Moreover, we conclude that there is overlapping function for ADF and n-cofilin in presynaptic physiology, and compensation in single mutants. This is in perfect agreement with our previous observations of elevated synaptic n-cofilin levels in ADF mutants and, *vice versa*, increased synaptic ADF levels in n-cofilin mutants (Rust et al. 2010; Görlich et al. 2011). Functional redundancy of ADF and n-cofilin has been observed previously in cell culture experiments (Hotulainen et al. 2005), but it had not been reported in neurons and synapses before.

In line with previous *in vitro* studies (Zhou et al. 2004; Hotulainen et al. 2009; Gu et al. 2010), we recently demonstrated increased spine size in hippocampal pyramidal cells of n-cofilin mutants (Rust et al. 2010). Compared with n-cofilin mutants, spine size was enlarged in ACC mutants. This finding underlines the relevance of ADF/cofilin for spine morphology and provides evidence for a postsynaptic function of ADF. Apart from its role in structural plasticity, postsynaptic ADF/cofilin is relevant also for the mobility and synaptic recruitment of AMPA receptors (AMPARs; Gu et al. 2010; Rust et al. 2010; Wang et al. 2013). This ADF/cofilin function is not directly coupled to structural changes (Gu et al. 2010; Wang et al. 2013), thereby suggesting that ADF/cofilin controls different, temporally separated aspects of postsynaptic plasticity.

Our analyses of ADF/cofilin mutants revealed the capacity of n-cofilin to fully compensate for the loss of ADF in synapses, whereas ADF can only partially compensate the inactivation of n-cofilin. Thus, n-cofilin appears to be the major ADF/cofilin isoform in excitatory synapses, which is in agreement with its 6- to 10-fold higher abundance in brain lysates (Minamide et al. 2000). Although n-cofilin is also present in presynaptic terminals, it is predominantly located in spines (Racz and Weinberg 2006). In accordance with this, n-cofilin knockdown in culture, or inactivation in mice, impairs spine morphology and postsynaptic plasticity, but not presynaptic function (Hotulainen et al. 2009; Gu et al. 2010; Rust et al. 2010). The presence of ADF is therefore sufficient to compensate for the loss of n-cofilin in presynaptic terminals, but not in spines. We thus suggest that ADF is more relevant for presynaptic than for postsynaptic mechanisms, which is in agreement with a higher ADF concentration in presynaptic terminals compared with spines (Görlich et al. 2011). Taken together, our findings demonstrate that n-cofilin and ADF contribute equally well to presynaptic physiology, while n-cofilin is the limiting factor in postsynaptic plasticity.

Our study has demonstrated an increased number of docked vesicles and elevated levels of syntaxin 1-bound synaptobrevin 2 in ACC mice. These findings indicate defects in docking and priming of synaptic vesicles and strongly suggest a role for ADF/cofilin in neurotransmitter release. Several aspects of our study support this notion: first, the reduced PPR in ACC mice implies an increased vesicle release probability and/or a defect in the vesicle docking/priming machinery. Secondly, although the synapse density is reduced in the CA1 *stratum radiatum* of ACC mice, postsynaptic excitation upon Schaffer collateral stimulation is unchanged. Since unchanged mEPSC amplitudes demonstrate normal vesicular transmitter load and postsynaptic sensitivity in ACC mice, this effect can be explained only by an increased stimulation-induced neurotransmitter release. Thirdly, the IEI of mEPSCs inversely depends on the release probability of vesicles and the number of synapses (El-Husseini et al. 2000). The IEI was not altered in ACC mice, yet the synapse number was reduced. Therefore, the vesicle release probability is most likely increased in ACC mice. Hence, our data strongly suggest an important role of ADF/cofilin in vesicle exocytosis, which is in very good agreement with defective vesicle exocytosis upon genetic ablation of LIMK1 or slingshot, 2 regulators of ADF/cofilin activity (Meng et al. 2002; Yuen et al. 2010).

The decrease in "late phase" glutamate release from depolarized forebrain synaptosomes and the reduced postsynaptic responses upon sustained Schaffer collateral stimulation imply an important role of ADF/cofilin in vesicle recruitment to the active zone, apart from its function in vesicle exocytosis. From our data, we conclude that stabilization of the actin cytoskeleton impairs vesicle recruitment. On the other hand, pharmacological destabilization of the actin cytoskeleton increases vesicle mobility in cultured hippocampal neurons (Jordan et al. 2005). Hence, our data provide evidence for an inhibitory function of F-actin in vesicle mobilization in hippocampal CA3–CA1 synapses, similar to what was proposed for other synapses (Dillon and Goda 2005).

Our data suggest reduced synaptic actin depolymerization in ACC mice, which is in good agreement with the biochemical function of ADF and n-cofilin. Consequently, F-actin in synaptic structures from ACC mice is more stable as judged from the 2.3-fold increase in the F/G-actin ratio. We therefore conclude that ADF and n-cofilin are important regulators of actin dynamics in synapses. Profilin 2, an actin-binding protein that promotes actin polymerization by replenishing the pool of ATP-bound G-actin (Witke 2004), has been associated with synaptic actin dynamics (Pilo Boyl et al. 2007). Profilin 2 mutants display a block in activity-induced synaptic actin polymerization, contrary to the defect seen in ACC mice. Despite the contrasting results in synaptic actin dynamics, the resulting defects in presynaptic function are surprisingly similar in profilin 2 mutants and ACC mice. In both mutants, the number of docked vesicles and the level of syntaxin 1-bound synaptobrevin 2 are increased, and electrophysiological recordings demonstrated increased vesicle exocytosis. Based on the phenotype of profilin 2 mutants, it has been postulated that F-actin forms a barrier within presynaptic terminals which is required for regulating vesicle exocytosis (Pilo Boyl et al. 2007)—a conclusion that is in agreement with a reduced IEI of mEPSCs upon pharmacological blockade of actin polymerization (Morales et al. 2000; Shupliakov et al. 2002). Our analysis of ACC mice extends this view and paints a more detailed picture on the role of actin in vesicle exocytosis. We postulate that actin needs to be highly dynamic in order to fulfill its function in exocytosis, and that depolymerization (ACC mice) and polymerization (profilin 2 mutants) are both activities that ultimately result in the same readout: a "dynamic actin cycle." Hence, a "dynamic actin cycle" rather than simple net polymerization or depolymerization is critical for synapse physiology. This interesting hypothesis would explain the apparent discrepancy between the deletion of ADF/cofilin and proteins like profilin 2. If a "dynamic actin cycle" is the critical parameter, we have to consider the experimental setup and discuss the resulting data with regard to the kinetics rather than steady state of actin remodeling.

In summary, we here demonstrate (i) the relevance of ADF for synapse physiology, (ii) overlapping synaptic functions for

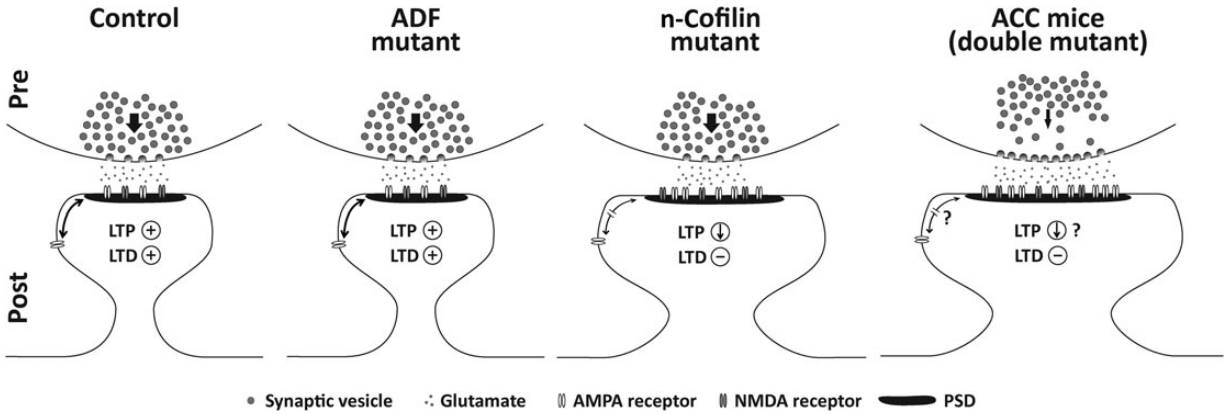

Figure 7. Model of ADF and n-cofilin function in hippocampal CA3–CA1 synapses. Inactivation of ADF alone has no adverse effect on synapse morphology or physiology. Conversely, inactivation of n-cofilin results in enlarged dendritic spines, impaired AMPAR mobility (indicated by a thinner double arrow), reduced long-term potentiation (LTP), and the absence of long-term depression (LTD), whereas presynaptic mechanisms remain fully preserved. The spine size is even further enlarged in ACC mice in which both ADF and n-cofilin are deleted. In ACC mice, the distribution of synaptic vesicles is altered and the number of docked vesicles is elevated. Moreover, vesicle recruitment is impaired (indicated by a thinner arrow in the presynaptic terminal), whereas vesicle exocytosis is increased (indicated by higher numbers of glutamate releasing vesicles). Future analysis will show to which extent AMPAR mobility, LTD, and LTP are impaired upon compound inactivation of ADF and n-cofilin.

ADF and n-cofilin, and (iii) the requirement of ADF/cofilin activity for presynaptic physiology. From our analyses of mutant mice, we propose the following model for ADF and n-cofilin function in excitatory synapses (Fig. 7): ADF and n-cofilin are both relevant for pre- and postsynaptic functions. However, genetic ablation of ADF does not interfere with synapse morphology or physiology. Conversely, inactivation of n-cofilin impairs postsynaptic mechanisms (spine size, AMPAR mobility, long-term potentiation, and long-term depression), but not presynaptic physiology. Impaired organization, mobilization, and exocytosis of synaptic vesicles become evident only upon inactivation of both proteins. Additionally, compared with n-cofilin mutants, spines are further enlarged in ACC. At this juncture, the defects in presynaptic physiology do not allow conclusions on the postsynaptic physiology in ACC mice. This will require genetic ablation of ADF/cofilin exclusively in CA1 pyramidal neurons.

Funding

This work was supported by the Research Initiative Membrane Transport (RIMB) of the University of Kaiserslautern and by the VIGONI Program of the German Academic Exchange Service (50756644). M.B.R. was supported by the Stiftung Rheinland-Pfalz für Innovation (961-386261/877).

Notes

We thank K. Ociepka and T. Kehrwald for excellent technical assistance, Dr L. Viltono for support with electron microscopy, Dr R. Klein for providing CaMKII-cre mice, Dr P. Soriano for providing Rosa26 cre reporter mice, and K. Rehklau, Dr J. Kullmann, and Dr P. Pilo Boyl for critical reading an early version of the manuscript. *Conflict of Interest*: The authors declare no competing financial interest.

References

Bellenchi GC, Gurniak CB, Perlas E, Middei S, Ammassari-Teule M, Witke W. 2007. N-cofilin is associated with neuronal migration disorders and cell cycle control in the cerebral cortex. Genes Dev. 21:2347–2357.

Bernstein BW, Bamburg JR. 2010. ADF/cofilin: a functional node in cell biology. Trends Cell Biol. 20:187–195.

Bernstein BW, Bamburg JR. 1989. Cycling of actin assembly in synaptosomes and neurotransmitter release. Neuron. 3:257–265.

Bosch M, Hayashi Y. 2011. Structural plasticity of dendritic spines. Curr Opin Neurobiol. 22:383–388.

Cingolani LA, Goda Y. 2008. Actin in action: the interplay between the actin cytoskeleton and synaptic efficacy. Nat Rev Neurosci. 9: 344–356.

Dillon C, Goda Y. 2005. The actin cytoskeleton: integrating form and function at the synapse. Ann Rev Neurosci. 28:25–55.

Dunkley PR, Jarvie PE, Robinson PJ. 2008. A rapid Percoll gradient procedure for preparation of synaptosomes. Nat Protoc. 3: 1718–1728.

El-Husseini AE, Schnell E, Chetkovich DM, Nicoll RA, Bredt DS. 2000. PSD-95 involvement in maturation of excitatory synapses. Science. 290:1364–1368.

Fifkova E, Delay RJ. 1982. Cytoplasmic actin in neuronal processes as a possible mediator of synaptic plasticity. J Cell Biol. 95: 345–350.

Fukazawa Y, Saitoh Y, Ozawa F, Ohta Y, Mizuno K, Inokuchi K. 2003. Hippocampal LTP is accompanied by enhanced F-actin content within the dendritic spine that is essential for late LTP maintenance in vivo. Neuron. 38:447–460.

Goodson M, Rust MB, Witke W, Bannerman D, Mott R, Ponting CP, Flint J. 2012. Cofilin-1: a modulator of anxiety in mice. PLoS Genet. 8:e1002970.

Görlich A, Wolf M, Zimmermann AM, Gurniak CB, Al Banchaabouchi M, Sassoe-Pognetto M, Witke W, Friauf E, Rust MB. 2011. N-Cofilin can compensate for the loss of ADF in excitatory synapses. PloS ONE. 6:e26789.

Gu J, Lee CW, Fan Y, Komlos D, Tang X, Sun C, Yu K, Hartzell HC, Chen G, Bamburg JR et al. 2010. ADF/cofilin-mediated actin dynamics regulate AMPA receptor trafficking during synaptic plasticity. Nat Neurosci. 13:1208–1215.

Herde MK, Friauf E, Rust MB. 2010. Developmental expression of the actin depolymerizing factor ADF in the mouse inner ear and spiral ganglia. J Comp Neurol. 518:1724–1741.

Hotulainen P, Llano O, Smirnov S, Tanhuanpaa K, Faix J, Rivera C, Lappalainen P. 2009. Defining mechanisms of actin polymerization and depolymerization during dendritic spine morphogenesis. J Cell Biol. 185:323–339.

Hotulainen P, Paunola E, Vartiainen MK, Lappalainen P. 2005. Actin-depolymerizing factor and cofilin-1 play overlapping roles in promoting rapid F-actin depolymerization in mammalian nonmuscle cells. Mol Biol Cell. 16:649–664.

Jordan R, Lemke EA, Klingauf J. 2005. Visualization of synaptic vesicle movement in intact synaptic boutons using fluorescence fluctuation spectroscopy. Biophys J. 89:2091–2102.
Korobova F, Svitkina T. 2010. Molecular architecture of synaptic actin cytoskeleton in hippocampal neurons reveals a mechanism of dendritic spine morphogenesis. Mol Biol Cell. 21:165–176.
Landis DM, Hall AK, Weinstein LA, Reese TS. 1988. The organization of cytoplasm at the presynaptic active zone of a central nervous system synapse. Neuron. 1:201–209.
McNair K, Spike R, Guilding C, Prendergast GC, Stone TW, Cobb SR, Morris BJ. 2010. A role for RhoB in synaptic plasticity and the regulation of neuronal morphology. J Neurosci. 30:3508–3517.
Meng Y, Zhang Y, Tregoubov V, Janus C, Cruz L, Jackson M, Lu WY, MacDonald JF, Wang JY, Falls DL et al. 2002. Abnormal spine morphology and enhanced LTP in LIMK-1 knockout mice. Neuron. 35:121–133.
Minamide LS, Striegl AM, Boyle JA, Meberg PJ, Bamburg JR. 2000. Neurodegenerative stimuli induce persistent ADF/cofilin-actin rods that disrupt distal neurite function. Nat Cell Biol. 2:628–636.
Minichiello L, Korte M, Wolfer D, Kuhn R, Unsicker K, Cestari V, Rossi-Arnaud C, Lipp HP, Bonhoeffer T, Klein R. 1999. Essential role for TrkB receptors in hippocampus-mediated learning. Neuron. 24:401–414.
Morales M, Colicos MA, Goda Y. 2000. Actin-dependent regulation of neurotransmitter release at central synapses. Neuron. 27:539–550.
Murthy VN, De Camilli P. 2003. Cell biology of the presynaptic terminal. Ann Rev Neurosci. 26:701–728.
Nicholls DG, Sihra TS, Sanchez-Prieto J. 1987. Calcium-dependent and -independent release of glutamate from synaptosomes monitored by continuous fluorometry. J Neurochem. 49:50–57.
Pilo Boyl P, Di Nardo A, Mulle C, Sassoe-Pognetto M, Panzanelli P, Mele A, Kneussel M, Costantini V, Perlas E, Massimi M et al. 2007. Profilin2 contributes to synaptic vesicle exocytosis, neuronal excitability, and novelty-seeking behavior. EMBO J. 26:2991–3002.
Racz B, Weinberg RJ. 2006. Spatial organization of cofilin in dendritic spines. Neuroscience. 138:447–456.
Rust MB, Gurniak CB, Renner M, Vara H, Morando L, Gorlich A, Sassoe-Pognetto M, Banchaabouchi MA, Giustetto M, Triller A et al. 2010. Learning, AMPA receptor mobility and synaptic plasticity depend on n-cofilin-mediated actin dynamics. EMBO J. 29:1889–1902.
Sacchetti P, Carpentier R, Segard P, Olive-Cren C, Lefebvre P. 2006. Multiple signaling pathways regulate the transcriptional activity of the orphan nuclear receptor NURR1. Nucleic Acids Res. 34:5515–5527.
Schratt GM, Tuebing F, Nigh EA, Kane CG, Sabatini ME, Kiebler M, Greenberg ME. 2006. A brain-specific microRNA regulates dendritic spine development. Nature. 439:283–289.
Shi Y, Pontrello CG, DeFea KA, Reichardt LF, Ethell IM. 2009. Focal adhesion kinase acts downstream of EphB receptors to maintain mature dendritic spines by regulating cofilin activity. J Neurosci. 29:8129–8142.
Shupliakov O, Bloom O, Gustafsson JS, Kjaerulff O, Low P, Tomilin N, Pieribone VA, Greengard P, Brodin L. 2002. Impaired recycling of synaptic vesicles after acute perturbation of the presynaptic actin cytoskeleton. Proc Natl Acad Sci USA. 99:14476–14481.
Sim AT, Herd L, Proctor DT, Baldwin ML, Meunier FA, Rostas JA. 2006. High throughput analysis of endogenous glutamate release using a fluorescence plate reader. J Neurosci Methods. 153:43–47.
Soriano P. 1999. Generalized lacZ expression with the ROSA26 Cre reporter strain. Nat Genet. 21:70–71.
Spector I, Shochet NR, Blasberger D, Kashman Y. 1989. Latrunculins—novel marine macrolides that disrupt microfilament organization and affect cell growth: I. Comparison with cytochalasin D. Cell Motil Cytoskeleton. 13:127–144.
Tavazoie SF, Alvarez VA, Ridenour DA, Kwiatkowski DJ, Sabatini BL. 2005. Regulation of neuronal morphology and function by the tumor suppressors Tsc1 and Tsc2. Nat Neurosci. 8:1727–1734.
Tsuji T, Miyoshi T, Higashida C, Narumiya S, Watanabe N. 2009. An order of magnitude faster AIP1-associated actin disruption than nucleation by the Arp2/3 complex in lamellipodia. PloS ONE. 4:e4921.
Wang Y, Dong Q, Xu XF, Feng X, Xin J, Wang DD, Yu H, Tian T, Chen ZY. 2013. Phosphorylation of cofilin regulates extinction of conditioned aversive memory via AMPAR trafficking. J Neurosci. 33:6423–6433.
Witke W. 2004. The role of profilin complexes in cell motility and other cellular processes. Trends Cell Biol. 14:461–469.
Yamada H, Padilla-Parra S, Park SJ, Itoh T, Chaineau M, Monaldi I, Cremona O, Benfenati F, De Camilli P, Coppey-Moisan M et al. 2009. Dynamic interaction of amphiphysin with N-WASP regulates actin assembly. J Biol Chem. 284:34244–34256.
Yang EJ, Yoon JH, Min DS, Chung KC. 2004. LIM kinase 1 activates cAMP-responsive element-binding protein during the neuronal differentiation of immortalized hippocampal progenitor cells. J Biol Chem. 279:8903–8910.
Yuen EY, Liu W, Kafri T, van Praag H, Yan Z. 2010. Regulation of AMPA receptor channels and synaptic plasticity by cofilin phosphatase Slingshot in cortical neurons. J Physiol. 588:2361–2371.
Zhou L, Jones EV, Murai KK. 2012. EphA signaling promotes actin-based dendritic spine remodeling through slingshot phosphatase. J Biol Chem. 287:9346–9359.
Zhou L, Martinez SJ, Haber M, Jones EV, Bouvier D, Doucet G, Corera AT, Fon EA, Zisch AH, Murai KK. 2007. EphA4 signaling regulates phospholipase Cgamma1 activation, cofilin membrane association, and dendritic spine morphology. J Neurosci. 27:5127–5138.
Zhou Q, Homma KJ, Poo MM. 2004. Shrinkage of dendritic spines associated with long-term depression of hippocampal synapses. Neuron. 44:749–757.